Clinical Neurophysiology 131 (2020) 1252–1266

Contents lists available at ScienceDirect

Clinical Neurophysiology

journal homepage: www.elsevier.com/locate/clinph

Evaluation of neural activity by magnetospinography with 3D sensors

Kyohei Sakaki [a,1], Yuko Hoshino [b,1], Shigenori Kawabata [a,b,*], Yoshiaki Adachi [c], Taishi Watanabe [d], Kensuke Sekihara [b], Senichi Ishii [a], Masaki Tomori [a], Shoji Tomizawa [a], Mitsuhiro Enomoto [a], Atsushi Okawa [a]

[a] Department of Orthopedic Surgery, Tokyo Medical and Dental University, 1-5-45 Yushima, Bunkyo-ku, Tokyo 113-8510, Japan
[b] Department of Advanced Technology in Medicine, Graduate School of Tokyo Medical and Dental University, 1-5-45 Yushima, Bunkyo-ku, Tokyo 113-8510, Japan
[c] Applied Electronics Laboratory, Kanazawa Institute of Technology, Kanazawa-shi, Ishikawa 920-1331, Japan
[d] Healthcare Business Group, RICOH COMPANY, LTD., 2-3-10 Kandasurugadai Chiyoda-ku, Tokyo 101-0062, Japan

ARTICLE INFO

Article history:
Accepted 15 February 2020
Available online 19 March 2020

Keywords:
Magnetospinography
Magnetoneurography
Neuromagnetography
Spinal cord evoked magnetic field
Spinal cord evoked potential
Lumbar spinal canal
SQUID
Spatial filter

HIGHLIGHTS

- Magnetospinography with 3D sensors visualizes neural activity at depolarization sites.
- Action currents can be reconstructed from spinal cord evoked magnetic fields.
- Reconstructed currents at depolarization sites can localize spinal cord lesions.

ABSTRACT

Objective: Magnetospinography (MSG) has been developed for clinical application and is expected to be a novel neurophysiological examination. Here, we used an MSG system with sensors positioned in three orthogonal directions to record lumbar canal evoked magnetic fields (LCEFs) in response to peripheral nerve stimulation and to evaluate methods for localizing spinal cord lesions.
Methods: LCEFs from the lumbar area of seven rabbits were recorded by the MSG system in response to electrical stimulation of a sciatic nerve. LCEFs and lumbar canal evoked potentials (LCEPs) were measured before and after spinal cord compression induced by a balloon catheter. The lesion positions were estimated using LCEPs and computationally reconstructed currents corresponding to the depolarization site.
Results: LCEFs were recorded in all rabbits and neural activity in the lumbar spinal cord could be visualized in the form of a magnetic contour map and reconstructed current map. The position of the spinal cord lesion could be estimated by the LCEPs and reconstructed currents at the depolarization site.
Conclusions: MSG can visualize neural activity in the spinal cord and localize the lesion site.
Significance: MSG enables noninvasive assessment of neural activity in the spinal canal using currents at depolarization sites reconstructed from LCEFs.

1. Introduction

Multimodal assessment, including imaging techniques and electrophysiological examinations, is required for the diagnosis of nervous system diseases. Particularly for the spinal cord, functional examination with high temporal and spatial resolution is necessary, given that this region contains many different pathways in a relatively small area.

Electrophysiological examination of the spinal cord has been used not just for diagnosis, but also for intraoperative monitoring and preoperative assessment. However, electrophysiological recording is not always suitable for examining deep and complex structures such as the spinal cord, spinal nerve, and brachial

Abbreviations: CV, conduction velocity; LCEF, lumbar canal evoked magnetic field; LCEP, lumbar canal evoked potential; MEG, magnetoencephalography; MNG, magnetoneurography; MSG, magnetospinography; RENS, recursive null-steering; SQUID, superconducting quantum interference device; SD, standard deviation.

* Corresponding author at: Department of Advanced Technology in Medicine, Graduate School of Tokyo Medical and Dental University, 1-5-45 Yushima, Bunkyo-ku, Tokyo 113-8510, Japan.

E-mail addresses: hoshino.atm@tmd.ac.jp (Y. Hoshino), kawabata.orth@tmd.ac.jp (S. Kawabata), taishi.watanabe@jp.ricoh.com (T. Watanabe), k-sekihara@nifty.com (K. Sekihara), enomoto.orth@tmd.ac.jp (M. Enomoto), okawa.orth@tmd.ac.jp (Atsushi Okawa).

[1] These authors contributed equally to this work.

https://doi.org/10.1016/j.clinph.2020.02.025
1388-2457/

plexus. Potentials recorded on the skin surface have relatively small amplitudes and are affected by the conductivity of the tissues surrounding the spinal cord (Kakigi et al., 1982; Yamada et al., 1982; Yamada, 2000). Furthermore, electrophysiological recording from the skin surface such as via somatosensory evoked potentials requires many electrodes to scan a wide area. The use of lumbar canal evoked potentials (LCEPs) recorded with an epidural electrode is one method for obtaining clearer and larger signals. Although helpful for intraoperative and preoperative examinations, insertion of an epidural electrode into the spinal canal has risks. Therefore, noninvasive but accurate examinations are required for functional assessment of the spinal cord.

Magnetoneurography (MNG) has been developed as one such method. When a nerve is electrically stimulated, intra-axonal currents generate evoked magnetic fields according to Biot-Savart law or Ampère's law (Supplementary Fig. S1a, b). Volume currents and corresponding magnetic fields are not generated if a nerve or a current source is not located in a conductor. However, when a nerve is located in a conductor, such as a biological body, depolarization generates volume currents that flow into and out of the nerve; such currents also produce magnetic fields (Supplementary Fig. S1c). The calculation of these complicated magnetic fields in a homogeneous conductor has been reported by Sarvas (1987) and Stenroos and Sarvas (2012). Such biomagnetic fields are so weak as to be nine orders of magnitude smaller than the geomagnetic field (Wijesinghe, 2010) but can be detected in a magnetically shielded room using sensitive magnetic sensors.

MNG has some advantages over electrophysiological examination. First, action currents at any point in the scanned area can be computationally reconstructed from recorded magnetic fields, and MNG does not require large electrode arrays to be placed on the skin surface. Second, the magnetic field is not affected by the conductivity of the surrounding tissue. Therefore, action currents can be more precisely reconstructed from evoked magnetic fields than evoked potentials. Although magnetoencephalography (MEG) and magnetocardiography are already available for clinical use, magnetospinography (MSG) is now progressing to clinical application. The delay in the clinical application of MSG is mainly due to the features of the spinal cord. The evoked magnetic fields in the spinal cord are about one-tenth smaller than those of MEG and contain signals of different origins, including synaptic activities and propagating action currents. Therefore, signal localization in MSG is more difficult, and MSG needs a higher sampling rate and sensitivity.

We have reported neural activities in peripheral nerves and the spinal cord visualized by MNG and MSG in animals and humans, the propagation of lumbar canal evoked magnetic fields (LCEFs) (Hoshino et al., 2005; Kawabata et al., 2002; Ohkubo et al., 2003; Sumiya et al, 2017; Tomori et al., 2010), which are evoked magnetic fields in the lumbar spinal cord and cauda equina (Ishii et al., 2012; Tomizawa et al, 2008), and the physiological characteristics of action currents and magnetic fields in isolated nerves (Fukuoka et al., 2002, 2004). We have developed a superconducting quantum interference device (SQUID) magnetometer that simultaneously detects three directional components of magnetic fields, as well as improved artifact reduction methods and signal processing for better signal localization. Although we have already recorded LCEFs in human subjects (Sumiya et al., 2017), detailed neuromagnetic fields at the site of conduction blocks still need to be evaluated for the future clinical use of MSG. In our previous report, LCEFs at the site of cervical spinal cord compression in animals were recorded from the skin surface in response to spinal cord stimulation with an epidural catheter electrode (Tomori et al., 2010). In this report, we present LCEFs at compression sites of the lumbar spinal cord and cauda equina using less invasive sciatic nerve stimulation. In addition, we show that the lesion site was localized by the LCEFs or reconstructed currents at the depolarization site. The objectives of this study were to evaluate the effectiveness of MSG with 3D sensors for localizing lesion sites in the lumbar spinal canal and to demonstrate the feasibility of applying MSG in the clinical setting.

2. Methods

2.1. Animals and general measurement settings

Seven Japanese white rabbits (3.0–3.5 kg body weight) were used. First, the rabbits were anesthetized with ketamine chloride (25 mg/kg, intramuscular) and medetomidine chloride (0.1 mg/kg, subcutaneous). Intravenous ketamine chloride (20 mg/kg/h), medetomidine chloride (0.1 mg/kg/h), and vecuronium bromide (0.3 mg/kg/h) were administered to maintain anesthesia and muscle relaxation. Artificial ventilation was performed through a tracheotomy tube and electrocardiograms were continuously monitored during the procedure. LCEFs and LCEPs in response to sciatic nerve stimulation were respectively recorded before and after the spinal cord compression. After all recordings were finished, the animals were euthanized by intravenous infusion of pentobarbital (120 mg/kg). All procedures in this study were approved by the Animal Care Committee of Tokyo Medical and Dental University and carried out in accordance with EU Directive 2010/63/EU for animal experiments.

The correspondence of LCEFs and LCEPs was analyzed, and action currents were computationally reconstructed from LCEFs. In this study, we defined action currents as currents generated by nerve excitation, including intra-axonal currents and volume currents. In addition, the positions of the spinal cord compression were estimated by the LCEPs and reconstructed currents generated at the depolarization site.

2.2. Electrical stimulation

A unilateral sciatic nerve was exposed at the popliteal fossa and electrically stimulated (60 Hz; monophasic square waves; 0.03 ms width; 5–10 mA constant current, above the motor threshold) using a bipolar electrode. We used high-frequency stimulation to suppress synaptic activity. Electrical stimulation and recording of LCEPs were done by the MEB2200 electromyogram/evoked potential measuring system (Nihon Koden, Tokyo, Japan). For measurement of LCEFs, the nerves were electrically stimulated in the same manner.

2.3. Measurement of LCEPs

A five-pole catheter electrode (15-mm intervals; Unique Medical, Tokyo, Japan) was inserted into the lumbar epidural space through a 3-mm-diameter hole made at the caudal end of the sacrum (Fig. 1). The LCEPs before and after the spinal cord compression were recorded from the five poles of the epidural electrode at a sampling rate of 10 kHz with 100 Hz to 5 kHz bandpass filtering. A reference electrode was placed at the ear. An average of 50 to 100 responses was analyzed at each point. During the spinal cord compression procedure, LCEPs were continuously recorded to confirm that the peak amplitude decreased to lower than 50%. The position of the catheter electrode was obtained by X-ray imaging (Fig. 2).

2.4. Measurement of LCEFs

All recordings were performed in a magnetically shielded room using the MSG system, a 120-channel SQUID biomagnetometer system developed by the Applied Electronics Laboratory, Kana-

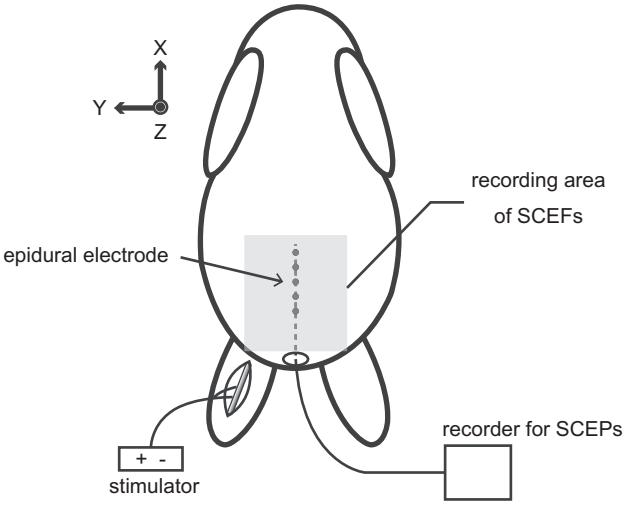

Fig. 1. Rabbits and measurement setting. After a rabbit was anesthetized, a five-pole catheter electrode was inserted into the lumbar epidural space through a 3-mm-diameter hole made at the caudal end of the sacrum. A unilateral sciatic nerve was electrically stimulated, and LCEPs were recorded from the catheter electrode. The shaded square represents the recording area of LCEFs. The coordinates were set as illustrated. LCEP: lumbar canal evoked potential; LCEF: lumbar canal evoked magnetic field.

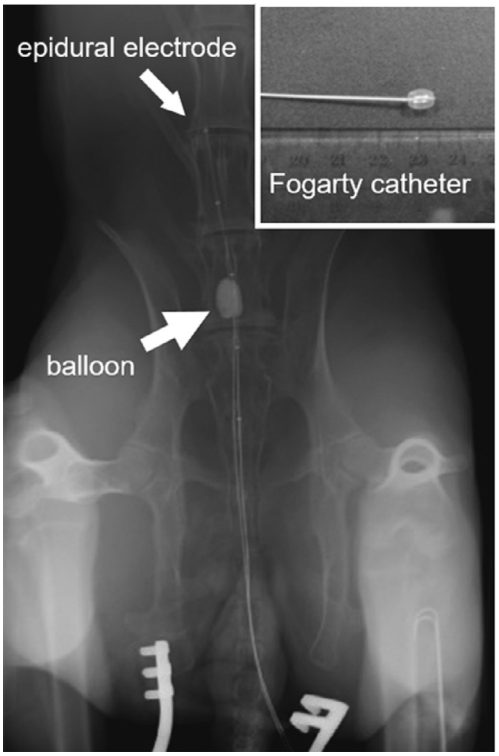

Fig. 2. X-ray image of the lumbar spine and sacrum with a catheter electrode and Fogarty catheter. A catheter electrode is inserted into the lumbar spinal canal to record LCEPs. A Fogarty catheter with a 6-mm-diameter balloon (Edwards Lifesciences, Irvine, CA) is advanced to the level of the L7 vertebra to exert spinal cord compression. LCEP: lumbar canal evoked potential.

zawa Institute of Technology (Adachi et al., 2009). The sensor array is composed of 40 SQUID magnetic flux sensors arranged in an eight-by-five matrix-like configuration at 20-mm intervals (Fig. 3). Each sensor is a vector-type gradiometer that contains three pickup coils (X, Y, and Z coils) positioned orthogonally to one another to simultaneously detect three directional components of magnetic fields (Fig. 3b). The X coil is defined to detect magnetic fields in the X direction (X axis), the Y coil detects magnetic fields in the Y direction (Y axis), and the Z coil magnetic fields in the Z direction (Z axis). The baseline length of the gradiometric pickup coils is extended to 68 mm to be optimized for the deep magnetic sources in the spinal cord. The typical noise level of the SQUID sensors was less than 5 $fT/Hz^{1/2}$ at 1 kHz.

Rabbits were placed on the biomagnetometer system in the supine position, ensuring that the spine was parallel to the X axis and that the body surface was parallel to the X–Y plane (Fig. 4). LCEFs were recorded while leaving the dorsal skin surface and spine intact. The signals from each sensor were acquired at a sampling rate of 40 kHz, with 10 Hz to 5 kHz bandpass filtering. Approximately 6000 responses to electrical stimulation were averaged at each sensor. The number of averages was set as waveforms adequate for evaluation. Another similar measurement was made after the rabbit was moved 5 mm along the X axis, and LCEFs were measured eight times in total for each rabbit. Accordingly, signals from 320 different measurement points were obtained (Fig. 4c) and LCEFs were visualized as isomagnetic contour maps. After the spinal cord compression, LCEFs were recorded in the same manner.

Two marker coils that generate sinusoidal magnetic fields (8 mm in diameter and driven by a given current of 50–200 μA) were placed on the rabbit, and the positions of the marker coils in the measurement area were obtained (Erné et al., 1987). The relative positions of the marker coils, spinal column, and epidural electrode were determined from X-ray film (Fig. 5). Using this information, we obtained the position of the neural activity in the measurement area.

2.5. Signal processing

Raw data of the recorded LCEFs were first processed using an artifact reduction method, the dual signal subspace projection algorithm (Sekihara et al., 2016). Then, the position and intensity of current sources were reconstructed from the processed data using a spatial filter algorithm, the recursive null-steering (RENS) beamformer (Kumihashi and Sekihara, 2010; Sekihara and Nagarajan, 2015).

2.6. Model of the incomplete spinal cord compression

A Fogarty catheter with a 6-mm-diameter balloon (Edwards Lifesciences, Irvine, CA) was inserted into the lumbar epidural space through the same hole used for insertion of the epidural electrode. The tip of the catheter was advanced to the level of L6–7 vertebra, with the position confirmed using X-ray imaging (Fig. 2). The balloon was positioned between two poles of the epidural electrode, specifically the second and the third poles from the caudal side. In rabbits, the lumbar enlargement in the spinal cord contains the L4–7 and S1–3 spinal nerves that contribute to the lumbosacral plexus, including the sciatic nerve, and the spinal cord continues into the sacral vertebrae (Greenaway et al., 2001; Sohn and Couto, 2012). In the present study, the spinal cord compression was performed at the L6–7 vertebra.

After the position of the catheter was determined, contrast dye was injected to pressurize the spinal cord. The balloon (filled with contrast dye) was confirmed to be at L6–7 by X-ray (Fig. 2). The spinal cord compression was maintained until simultaneously recorded LCEPs decreased less than 50% in peak amplitude to induce incomplete injury. Following the recording of LCEFs after the spinal compression, LCEPs were recorded again to confirm that the amplitude loss had not recovered.

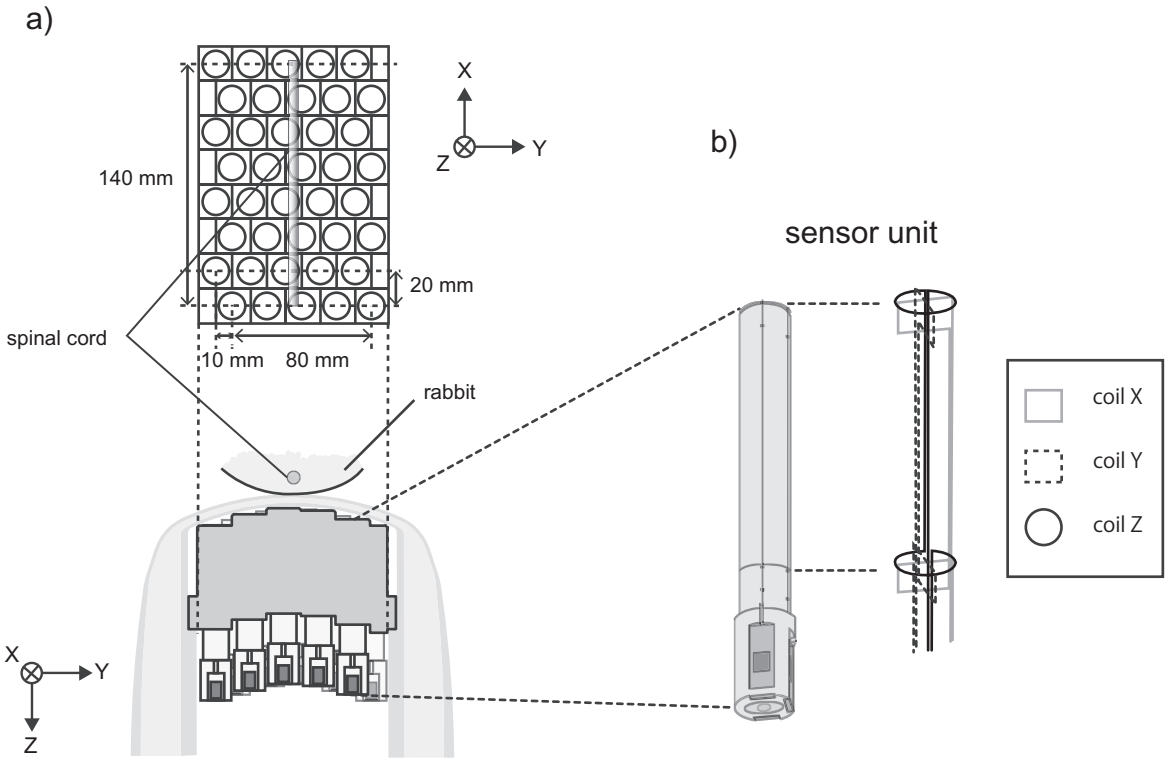

Fig. 3. The 120-channel SQUID biomagnetometer system (Applied Electronics Laboratory, Kanazawa Institute of Technology). (a) Overhead and side views of the sensor array. The sensor array is composed of 40 SQUID magnetic flux sensors arranged in an eight-by-five matrix-like configuration at 20-mm intervals. The rabbit is placed on the outer surface of the biomagnetometer system in the supine position. The spine and spinal cord are assumed to be parallel to the X axis and the body surface is parallel to the X–Y plane. (b) Each sensor is a vector-type gradiometer, which contains three pickup coils positioned orthogonally to one another (X, Y, and Z coils). Each sensor simultaneously detects magnetic fields in each corresponding direction (e.g., the X coil is defined to detect magnetic fields in the X direction).

2.7. Localization of the spinal cord compression

The positions of the lesion sites were estimated in the seven rabbits by analysis of LCEPs and reconstructed currents. The positions of the center of the balloon and the poles of the epidural electrode were obtained from X-ray film and marker coil localization; the stimulation side (caudal side) was assumed to be the negative direction in the X axis.

In the analysis of the LCEPs, we assumed that the level of the lesion site would be the midpoint of the two electrodes where the peak amplitude is decreased to less than 50% of the recording before the spinal cord compression. In addition, reconstructed currents flowing into the spinal canal were used to estimate the compression site. The lesion site was assumed to be the position where the current apparently was attenuated and decelerated. The purpose of this study was to localize the lesion site in the lumbar spinal canal by using the neural activity of the depolarization site. We used reconstructed currents flowing perpendicularly toward the spinal canal because they are supposed to be generated from depolarization, given their directions.

3. Results

3.1. LCEPs before and after spinal cord compression

LCEPs in response to sciatic nerve stimulation before and after spinal compression were recorded in all animals. The conduction velocities (CVs) of the LCEPs before the spinal cord compression—calculated from the peak latency—were 110.7 ± 16.5 m/s (mean ± standard deviation [SD], n = 7). The maximum peak-to-peak amplitude before the compression was 393.7 ± 203.4 μV (mean ± SD, n = 7). After the spinal cord compression, the LCEPs decelerated and were attenuated beyond the compression site (Fig. 5). Figs. 5–9 show results from the same subject.

3.2. LCEFs before and after spinal cord compression

LCEFs before and after spinal cord compression could be recorded in all rabbits. The LCEFs of a representative case in response to sciatic nerve stimulation obtained from the X, Y, and Z coils are shown in Fig. 6. The stimulation was on the positive side of the Y direction and the left side of the rabbit. In each coil, the upward waveform of the LCEFs indicates a positive direction in each axis. The LCEFs from coil X were magnetic fields almost parallel to the spinal cord. The amplitudes of the LCEFs from the X coils were generally larger on the contralateral side of the stimulation (e.g., the waveforms marked with asterisks in Fig. 6b). Coil Y picked up magnetic fields perpendicular to the spinal cord and the amplitude was larger near the spinal canal (see asterisks in Fig. 6c). In contrast, coil Z picked up vertical magnetic fields; the ventral-to-dorsal direction is positive in the rabbit. The polarity of LCEFs from Z coils was reversed for the right vs left sides of the spinal canal (e.g., asterisks in Fig. 6d).

Compared with the large LCEF waveforms before the spinal cord compression, those after the spinal cord compression decelerated or were attenuated in amplitude around the lesion site (e.g., red-rimmed waveforms in Fig. 6b and c, blue-rimmed waveforms in Fig. 6d).

Amplified waveforms of LCEFs from coil X before and after the spinal cord compression are shown in Fig. 6e. LCEFs recorded beside the spinal canal are shown because the magnetic fields from the X coil peaking above the volume currents flow into the spinal cord. These illustrated recording points are on the side opposite to the stimulation because the amplitudes of the LCEFs on the other side of the stimulation were larger, as described above. The

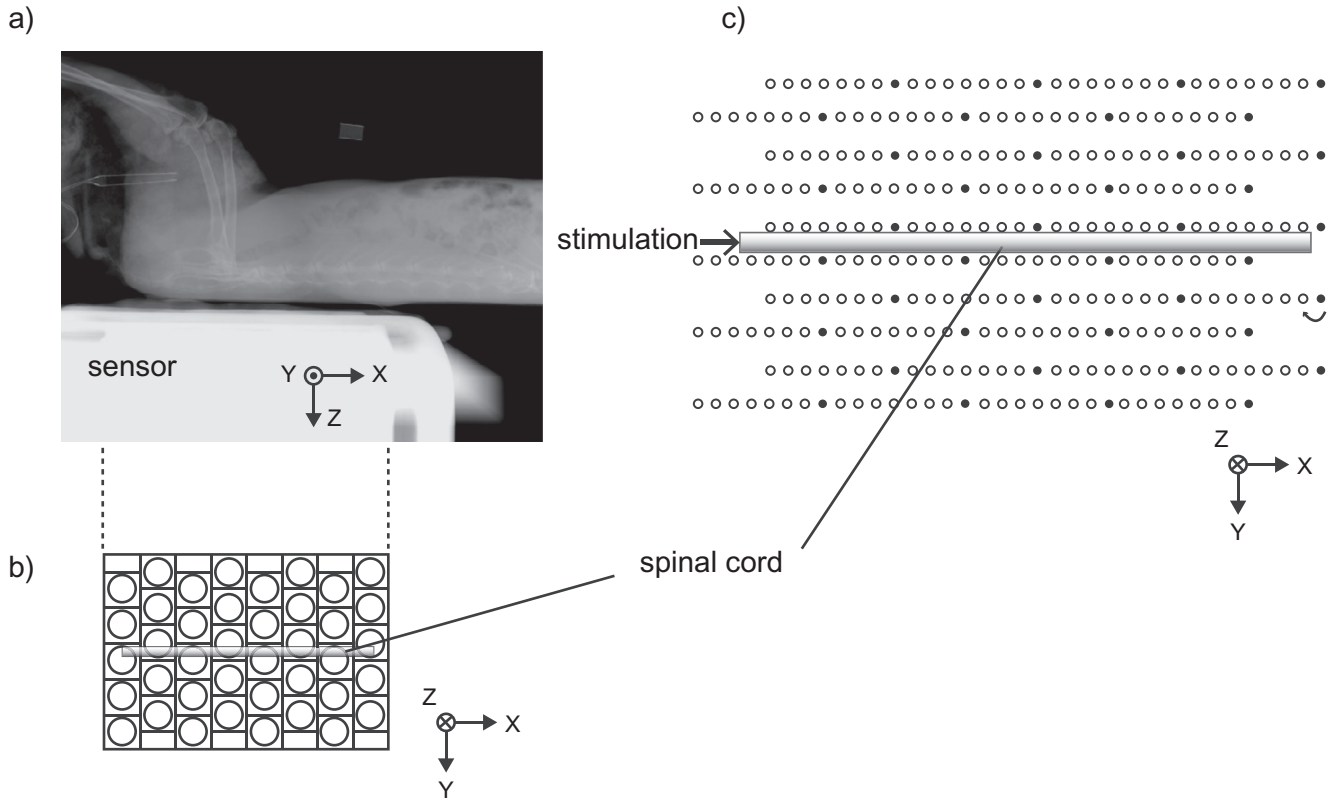

Fig. 4. Measurement area of LCEFs. (a) The rabbit is supine on the biomagnetometer system. (b) Overhead view (the ventral-to-dorsal direction in the animal) of the sensor array composed of 40 SQUID sensors. The spinal cord is assumed to be parallel to the X axis. (c) After one measurement of the LCEF, the rabbit was moved in the positive direction along the X axis and the LCEF recording was repeated. LCEFs were measured eight times in total for each rabbit. Accordingly, signals from 320 different measurement points were obtained. Black circles represent the first measurement points. LCEF: lumbar canal evoked magnetic field.

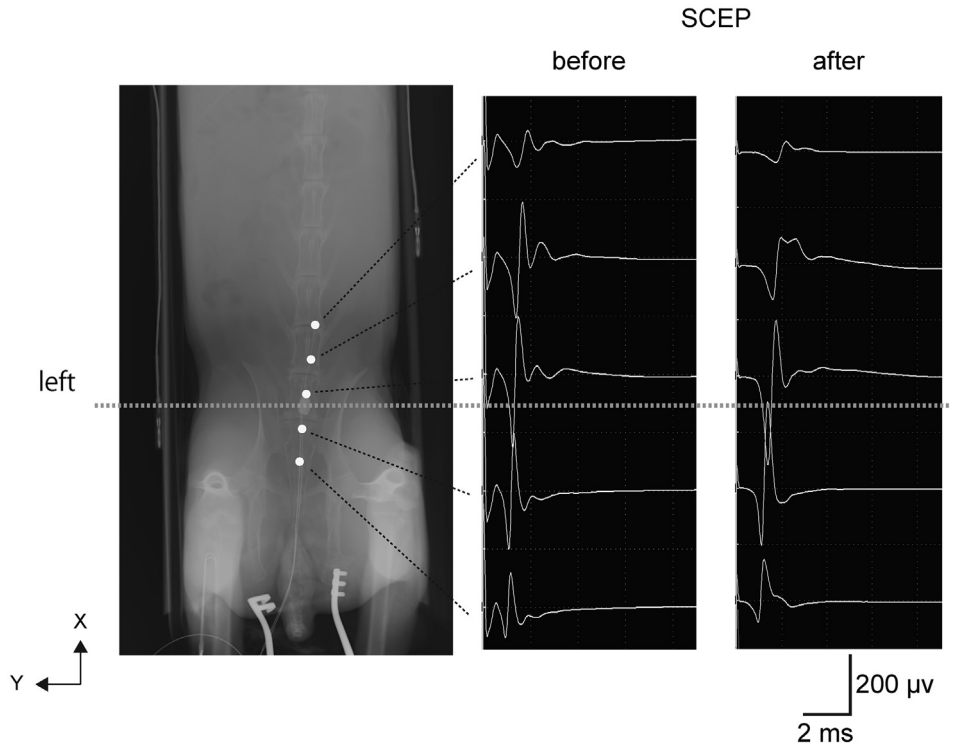

Fig. 5. LCEPs before and after the spinal compression. The X-ray image is shown in the dorsal-to-ventral direction of the animal. White circles in the X-ray image show the positions of the five poles of the catheter electrode. The dotted line means the center of the balloon used to compress the spinal cord. After the compression, the LCEPs decelerated and were attenuated at the pole second from cranial. Figs. 5–9 show results from the same subject. LCEP: lumbar canal evoked potential.

mean CV calculated from the peak latency of the LCEFs from coil X was 139.0 ± 13.3 m/s (mean ± SD, n = 7). The maximum peak-to-peak amplitude before the compression was 240.24 ± 58.27 fT (mean ± SD, n = 7). After the compression, the waveforms were attenuated near the lesion site.

The isomagnetic contour maps in Fig. 7 show the spatiotemporal transition of the LCEFs recorded from the X, Y, and Z coils before and after the spinal compression. The correspondence of the color in the contour map to the direction of the magnetic field is similar to that in Supplementary Fig. S1. In the contour map of the X coil (Fig. 7a), the red contour on the right side shows an X positive-directed magnetic field that is generated by currents flowing toward the spinal canal (starred area). After the compression, the red contour (starred area) was attenuated before the compression site. The LCEF from coil Y was highest above the spinal cord, and the magnetic field, illustrated as a red contour, was not evident in the contour map after the compression (Fig. 7b). In the contour map of the Z coil (Fig. 7c), the polarity of the magnetic fields was reversed on either side of the spinal cord. Before the compression, the leading magnetic field appeared from 1.0–1.4 ms. Because the left contour was red and the right one was blue, this magnetic field was generated by X positive-directed currents. Subsequently, the trailing magnetic field with reversed polarity appeared (1.6–2.0 ms), generated by X negative-directed currents. After the compression, the leading magnetic field decelerated, and the trailing magnetic field did not appear until 2.0 ms.

3.3. Reconstructed currents

The pseudocolor map and spatiotemporal transition of currents reconstructed from LCEFs by the spatial filter, the RENS beamformer, are shown in Fig. 8. In the pseudocolor map (Fig. 8a and b), arrows represent the direction of reconstructed currents and the color indicates the intensity of reconstructed currents (red is higher and blue is lower). Before the compression (Fig. 8a), caudal-to-cranial currents appeared and conducted cranially (1.0–1.5 ms) and opposite-directed currents conducted similarly (1.6–2.1 ms). After the compression (Fig. 8b), the leading currents appeared (1.0–1.7 ms) but were attenuated near the level of the spinal compression (dotted line). The trailing currents appeared at 2.0 ms but they did not pass beyond the compression site.

The blue circles in Fig. 8c are arbitrarily selected points to evaluate currents perpendicularly flowing toward the spinal canal. They are considered "virtual electrodes" and are numbered R1 to R10. These circles are at intervals of 5 mm and 10 mm away from the black line set as the center of the spinal canal. Because magnetic fields are generally larger on the other side of the stimulation, as described in Section 3.2, the blue circles are selected on the opposite side of the stimulation. Waveforms at blue circles indicate currents flowing perpendicular to the black line, and the direction toward the black line is upward in the waveform. Before the compression, the peak intensity of currents at blue circles was conducted in the caudal-to-cranial direction as time proceeded (Fig. 8c). However, after the spinal compression, the reconstructed currents decelerated and were attenuated around the level of the spinal cord compression (dotted line and R6 to R5 in Fig. 8c). The transition of the peak latency and the current density of the currents at the blue circles are shown in Fig. 8d. Changes in electrode R5 are apparent in both graphs.

3.4. Localization of the spinal cord compression

The positions of the lesion sites in the seven rabbits estimated by the LCEPs are shown in Fig. 9 (gray dots; mean ± SD, −0.88 ± 6.10 mm; n = 7). The lesion site is assumed to be the midpoint of two recording points where the LCEPs decreased more than 50% in peak amplitude. Similarly, the lesion sites in the seven rabbits estimated from the transition of reconstructed currents are shown as black dots (mean ± SD, 0.00 ± 4.50 mm; n = 7). The lesion site is assumed to be where the positive peak of reconstructed currents flowing perpendicularly toward the conduction pathway decelerated and was attenuated (as shown in Fig. 8d). As described in Sections 3.2 and 3.3, currents on the opposite side of the stimulation and flowing perpendicular toward the spinal canal were evaluated.

4. Discussion

MSG successfully visualized LCEFs in three directions as contour maps in response to sciatic nerve stimulation before and after spinal cord compression. As described in the Introduction, LCEFs

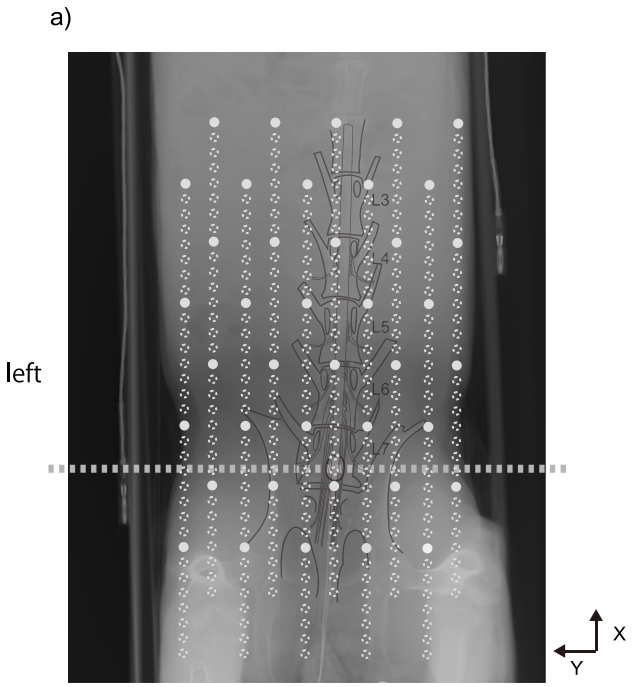

Fig. 6. (a) Measurement points and a schematic illustration of the lumbar spine and the spinal cord are overlaid on an X-ray image shown in the dorsal-to-ventral direction of the animal. Gray circles represent the first measurement points. The dotted line represents the center of the balloon. The stimulation is on the positive side of the Y axis (the left side of the rabbit). (b), (c) and (d) LCEFs before and after the spinal compression recorded from the sensors corresponding to the gray circles in (a). Recordings on the left side of the figure are before the compression and those on the right side are after the compression. Sensors out of order show a flat line. The spinal canal is located near the sixth columns from the left. (b) Left: LCEFs from X coils are generally larger on the opposite side of the stimulation (the negative side of the Y axis, the right side of the spinal canal). The signals on the right side of the spinal canal (asterisks) are larger than those on the left side. After the spinal cord compression, LCEFs on the right were decelerated and attenuated around the compression level compared with those on the left (e.g., red-rimmed waveforms). (c) LCEFs from Y coils. The signals near the spinal canal are larger than those on the right and left sides of the spinal canal (asterisks). The signals decelerated after the spinal cord compression (e.g., red-rimmed waveforms). (d) LCEFs from Z coils. The polarity of the waveforms is reversed for the right vs left sides of the spinal canal (asterisks). The attenuation or deceleration after the spinal cord compression is also detectable (e.g., blue-rimmed waveforms). (e) LCEFs recorded from the X coil and localization of the lesion site. Waveforms of LCEFs recorded from the X coil before and after the spinal compression. The stimulation is on the positive side of the Y axis (the left side of the rabbit). Filled white circles represent the poles of the epidural electrode. Gray dotted circles represent 320 recording points of LCEFs, and blue circles are selected to show LCEFs near the lesion site. Blue circles are not immediately above but lateral to the spinal canal because the magnetic fields from the X coil are maximal above the volume currents flowing into the spinal cord. After the compression, the waveforms were attenuated near the lesion site. LCEF: lumbar canal evoked magnetic field.

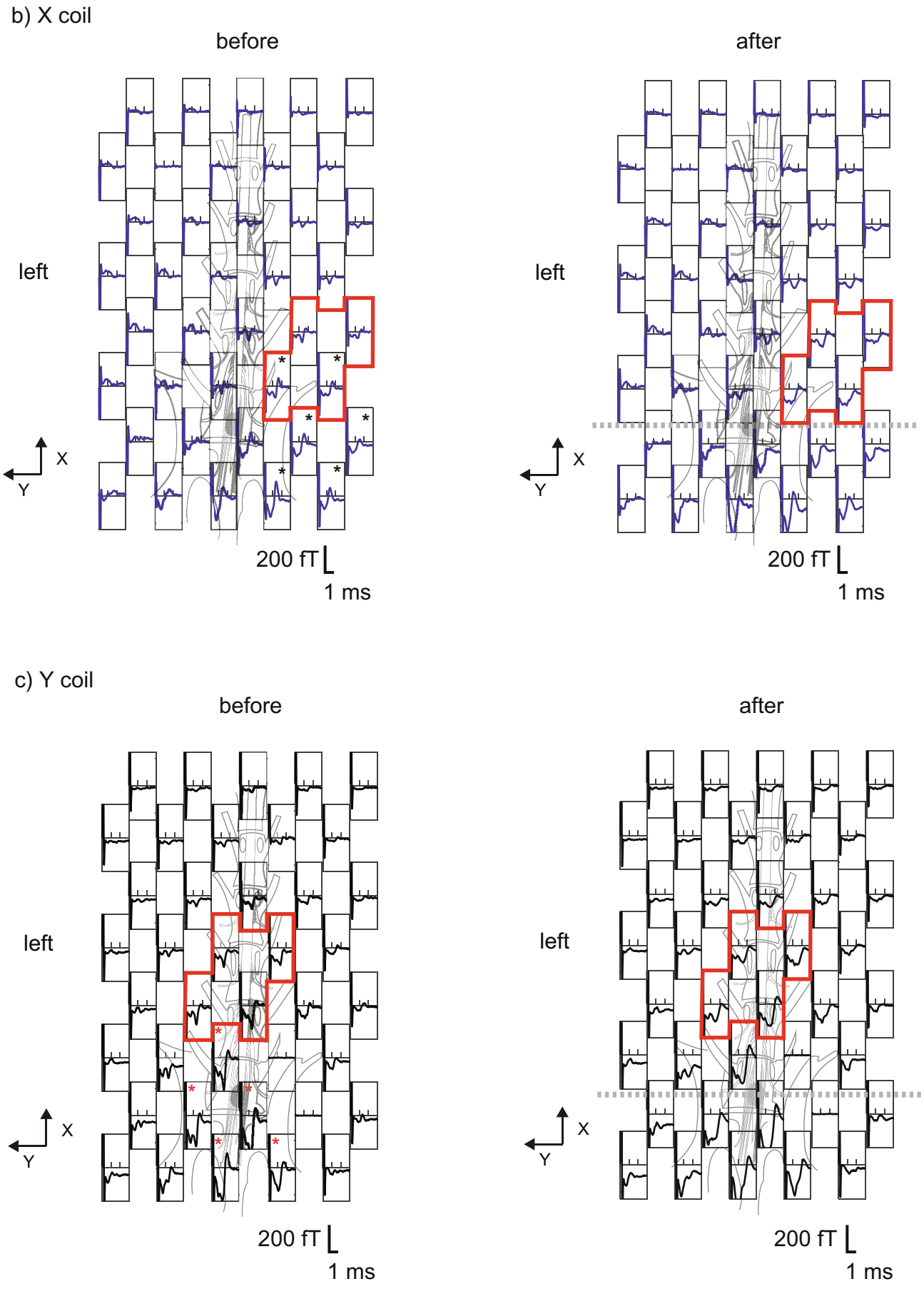

Fig. 6 (*continued*)

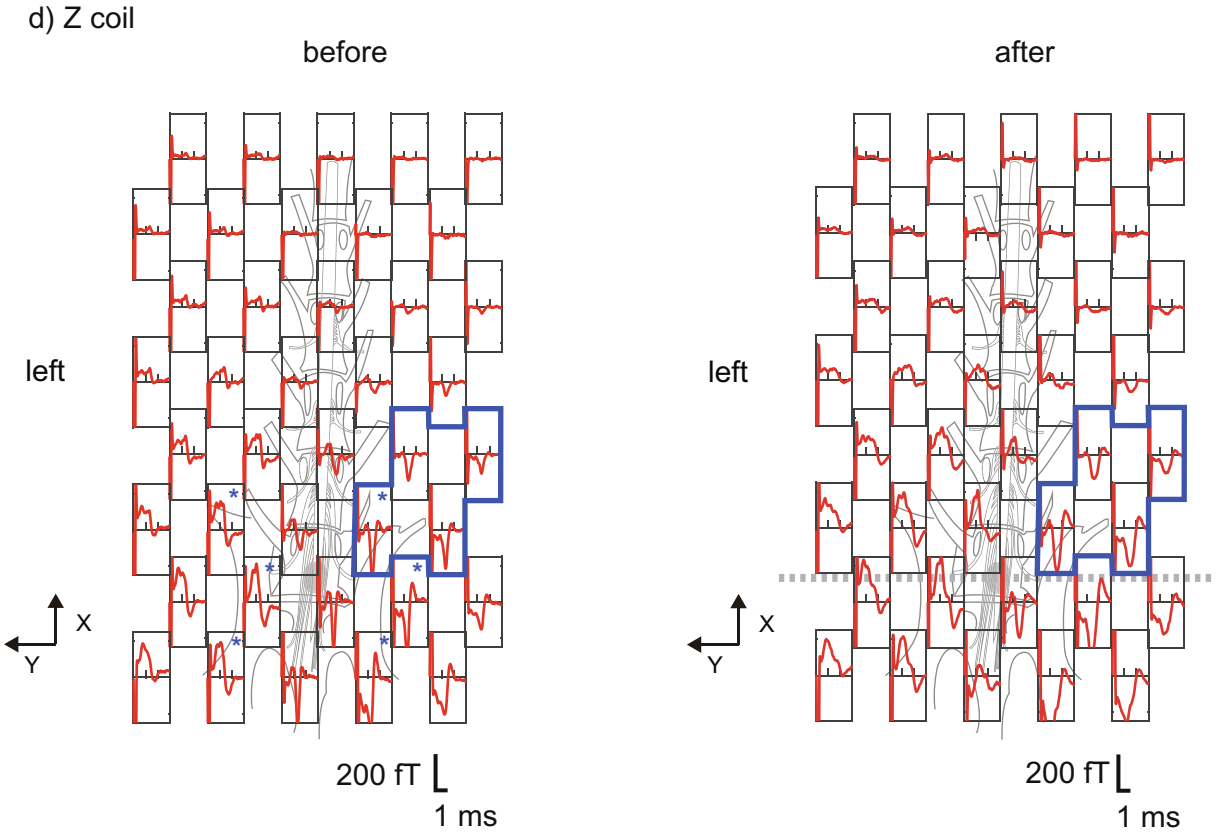

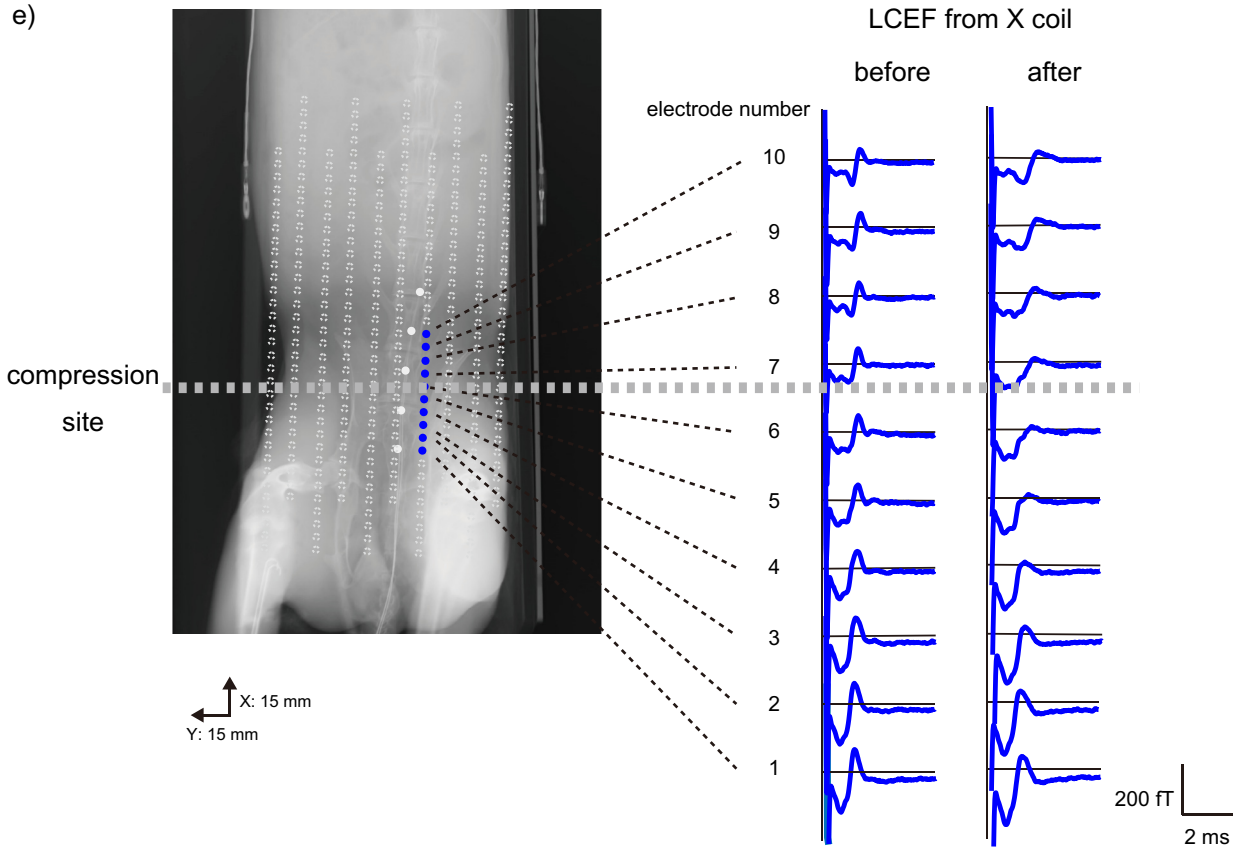

Fig. 6 (*continued*)

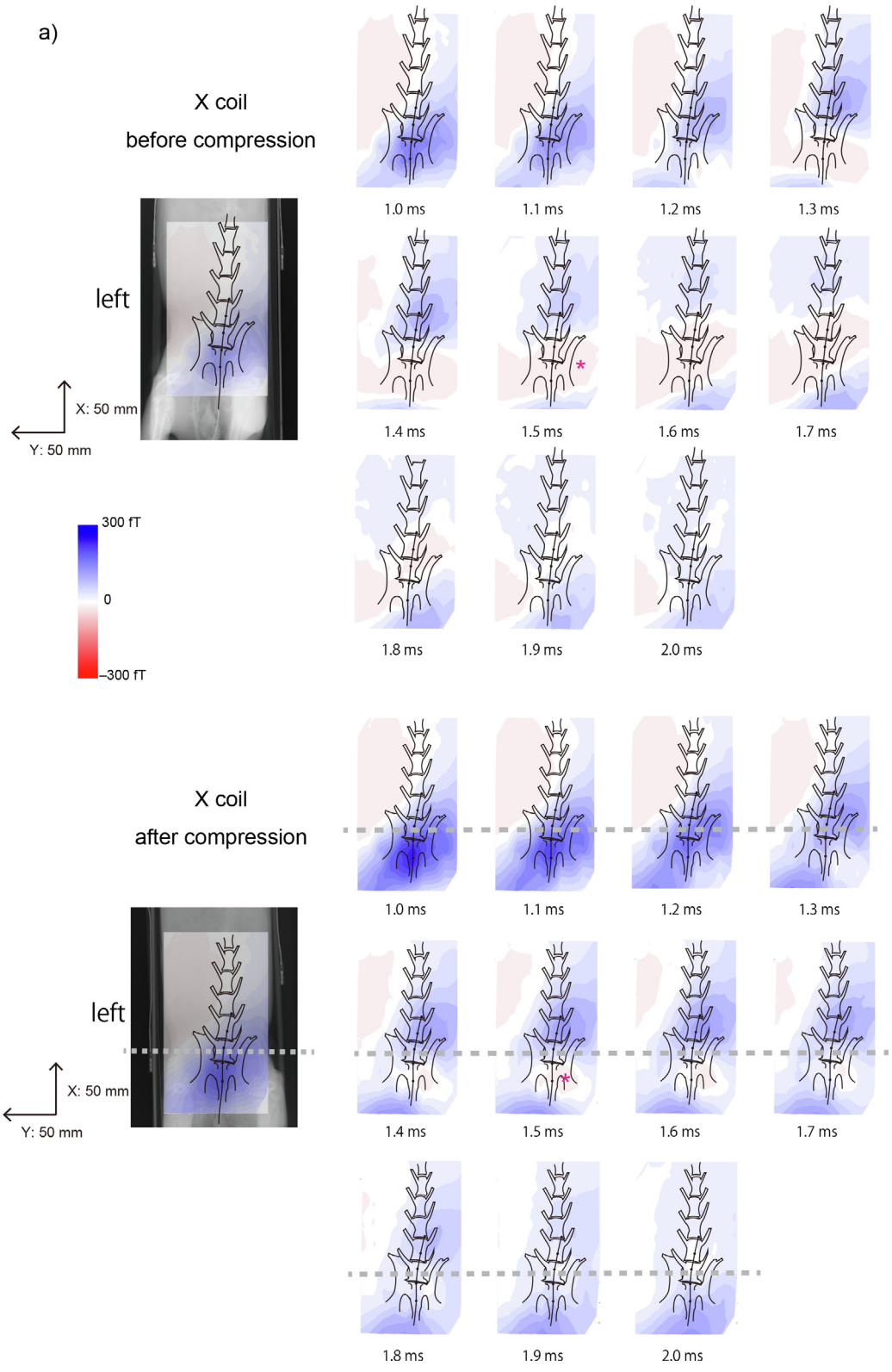

Fig. 7. Magnetic contour maps illustrated by LCEFs from the X, Y and Z coils. The X-ray image and contour maps are shown in the dorsal-to-ventral view. The left side of the figure corresponds to the left side of the rabbit. In the contour map, red indicates magnetic fields in the positive direction of each axis, and blue indicates negative. The correspondence of the color in the contour map to the direction of the magnetic field is similar to that of Supplementary Fig. S1. The stimulation is on the positive side of the Y axis, the left side of the rabbit. (a) Contour maps of LCEFs from the X coil before and after the spinal compression. The red contour (starred) shows an X positive-directed magnetic field. After the compression, the red contour was attenuated before the compression site. (b) Contour map of the Y coil. The LCEF is maximum above the spinal cord, and the magnetic field illustrated as a red contour did not appear in the contour map after the compression. (c) Contour map of the Z coil. The polarity of the magnetic fields is reversed on either side of the spinal cord. Before the compression, the leading magnetic field, which is depicted as a pair of positive and negative magnetic fields, appeared from 1.0–1.4 ms. Subsequently, the trailing magnetic field with reversed polarity appeared (1.6–2.0 ms). After the compression, the leading magnetic field decelerated and the trailing magnetic field did not appear until 2.0 ms. LCEF: lumbar canal evoked magnetic field.

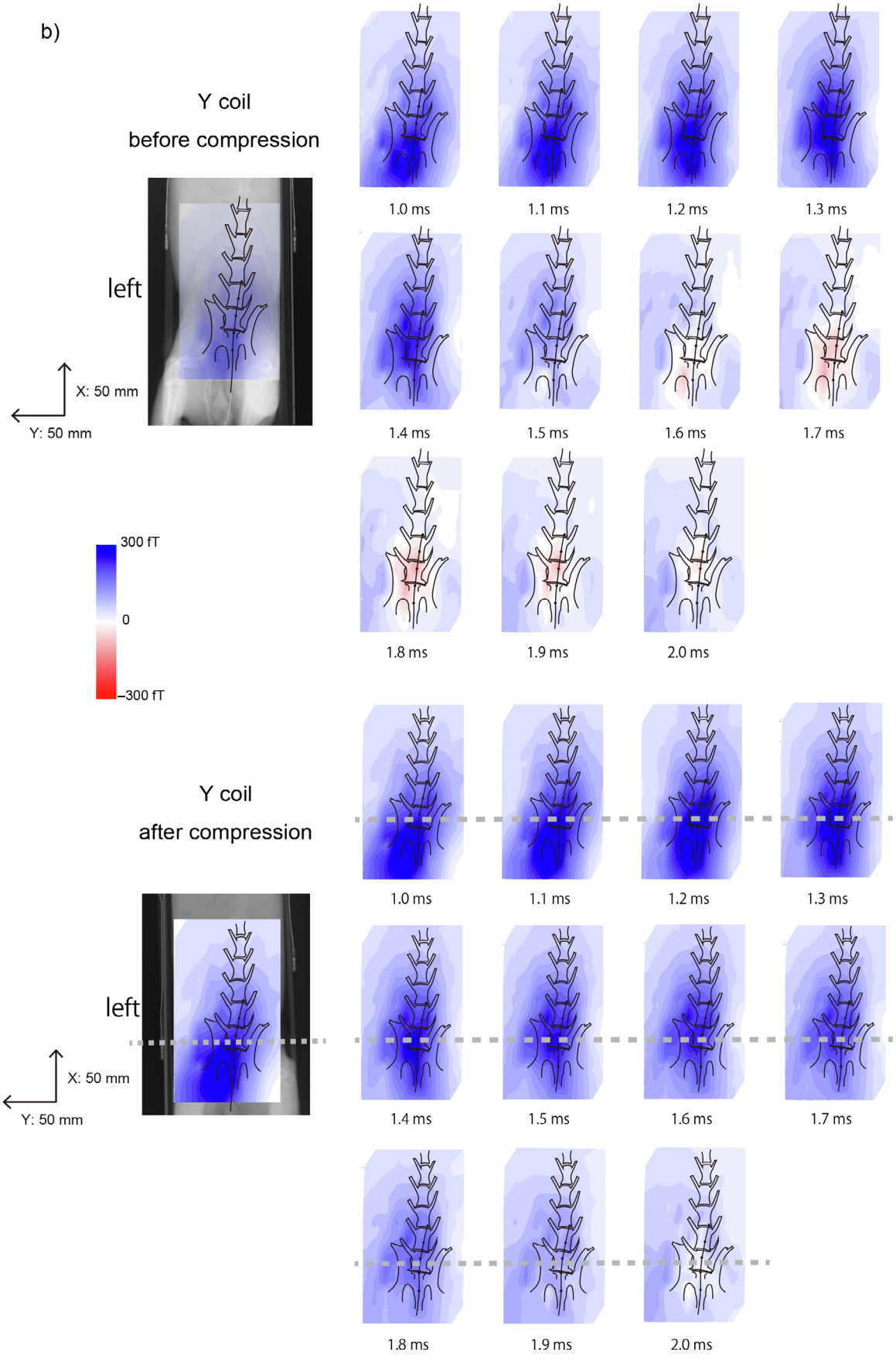

Fig. 7 (*continued*)

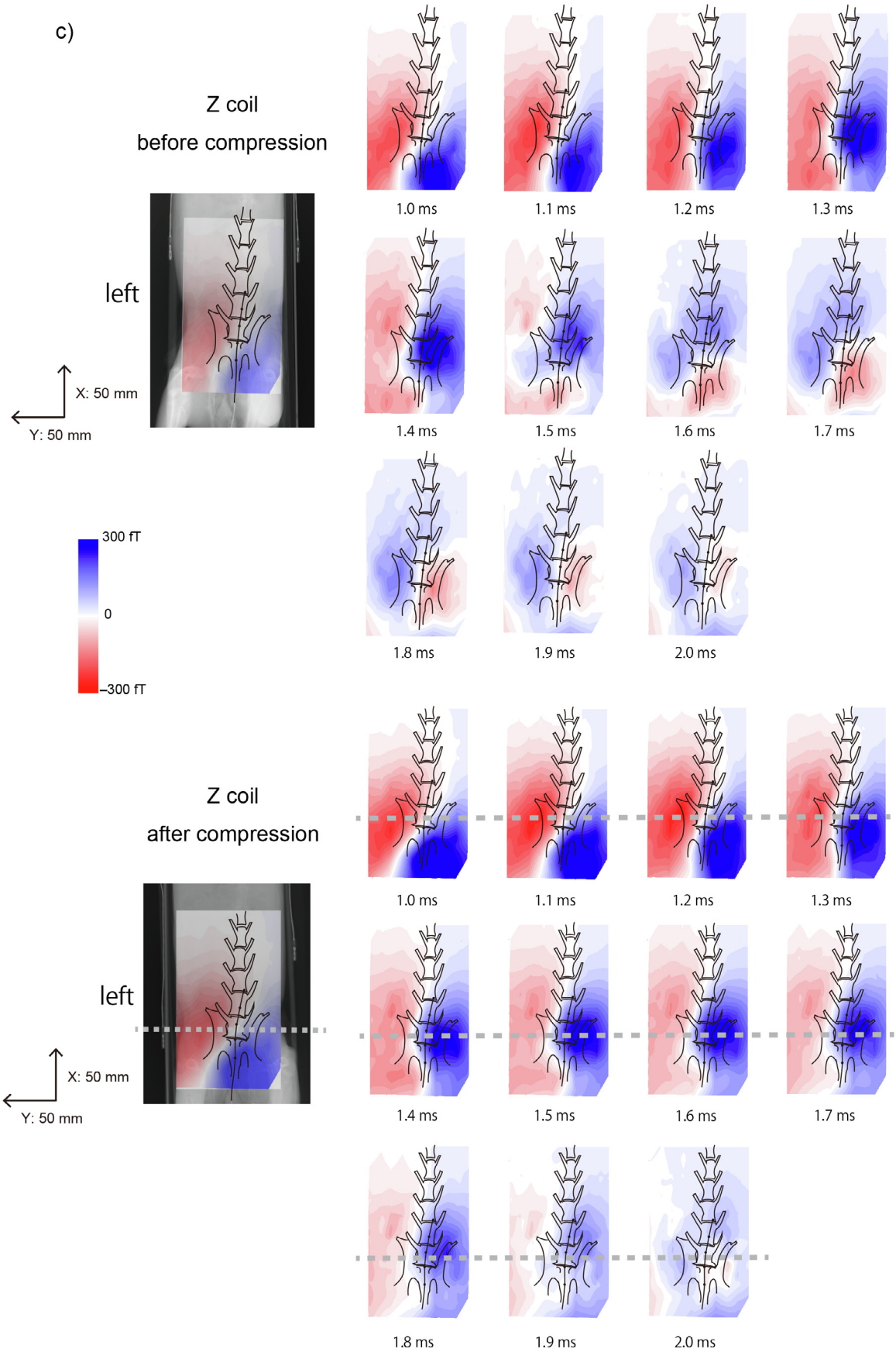

Fig. 7 (*continued*)

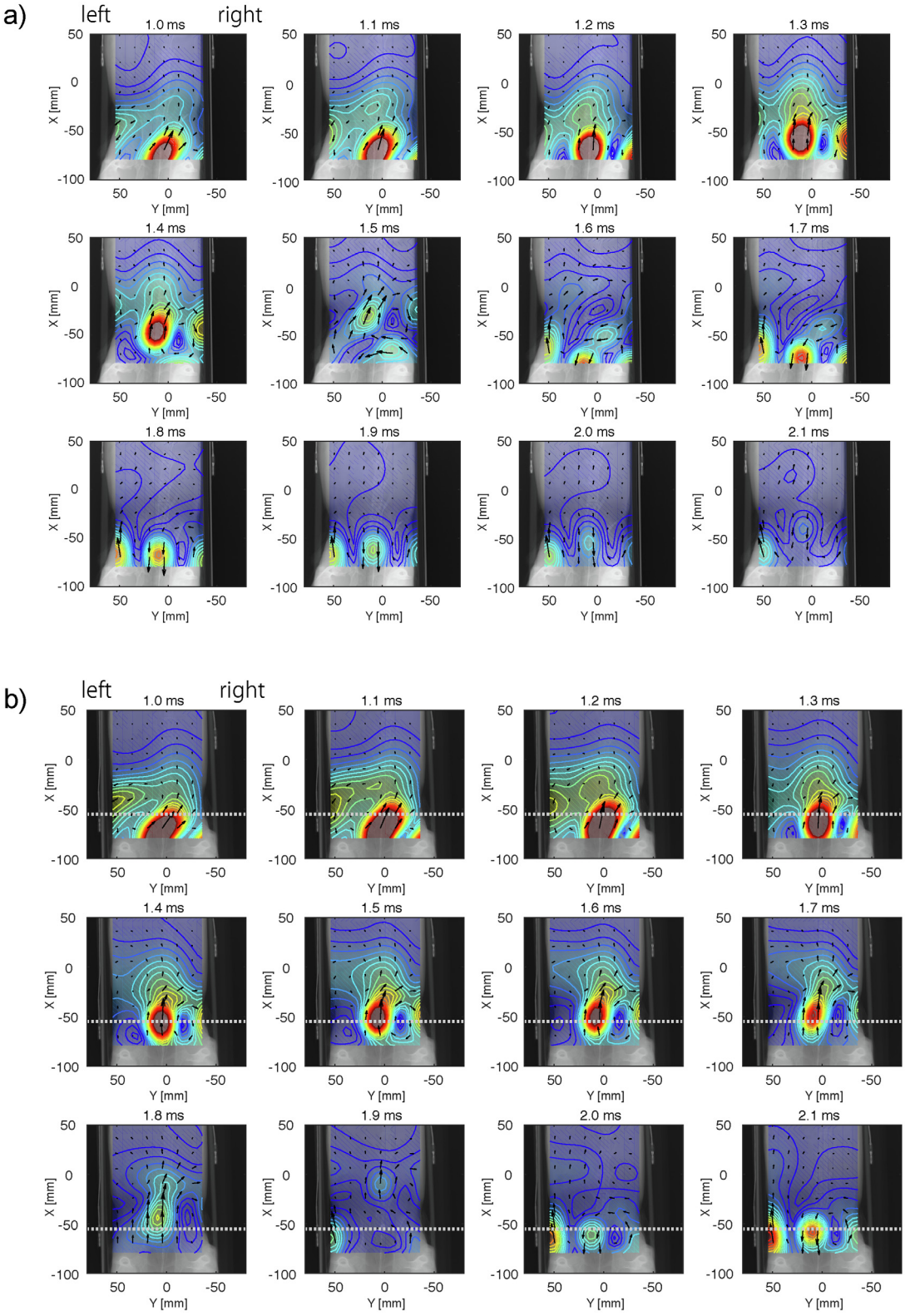

Fig. 8. Currents reconstructed from LCEFs before and after the spinal compression. (a) Reconstructed current map before the spinal compression. Caudal-to-cranial–directed currents appeared and conducted cranially (1.0–1.5 ms) and opposite-directed currents appeared and conducted similarly (1.6–2.1 ms). The stimulation is on the positive side of the Y axis. (b) Reconstructed current map after the spinal compression. Dotted lines show the spinal compression site. The leading currents appeared but decelerated and were attenuated near the dotted line (1.0–1.7 ms). The trailing currents appeared at 2.0 ms and were attenuated before the dotted line. (c) Waveform of reconstructed currents before and after the compression. Dotted lines show the spinal compression site. Blue circles (numbered from R1 to R10) are arbitrarily selected points at 5-mm intervals and 10 mm away from the black line representing the center of the spinal canal. Waveforms at blue circles indicate the density of currents perpendicularly flowing toward the black line. Before the spinal compression, the peak intensity of the currents conducted in the caudal-to-cranial direction. After the compression, these currents decelerated and were attenuated around the lesion site. (d) Spatiotemporal transition of the peak latency and current density of reconstructed currents at the blue circles in Fig. 8c (numbered R1 to R10). There are clear changes at electrode R5 in both graphs. LCEF: lumbar canal evoked magnetic field.

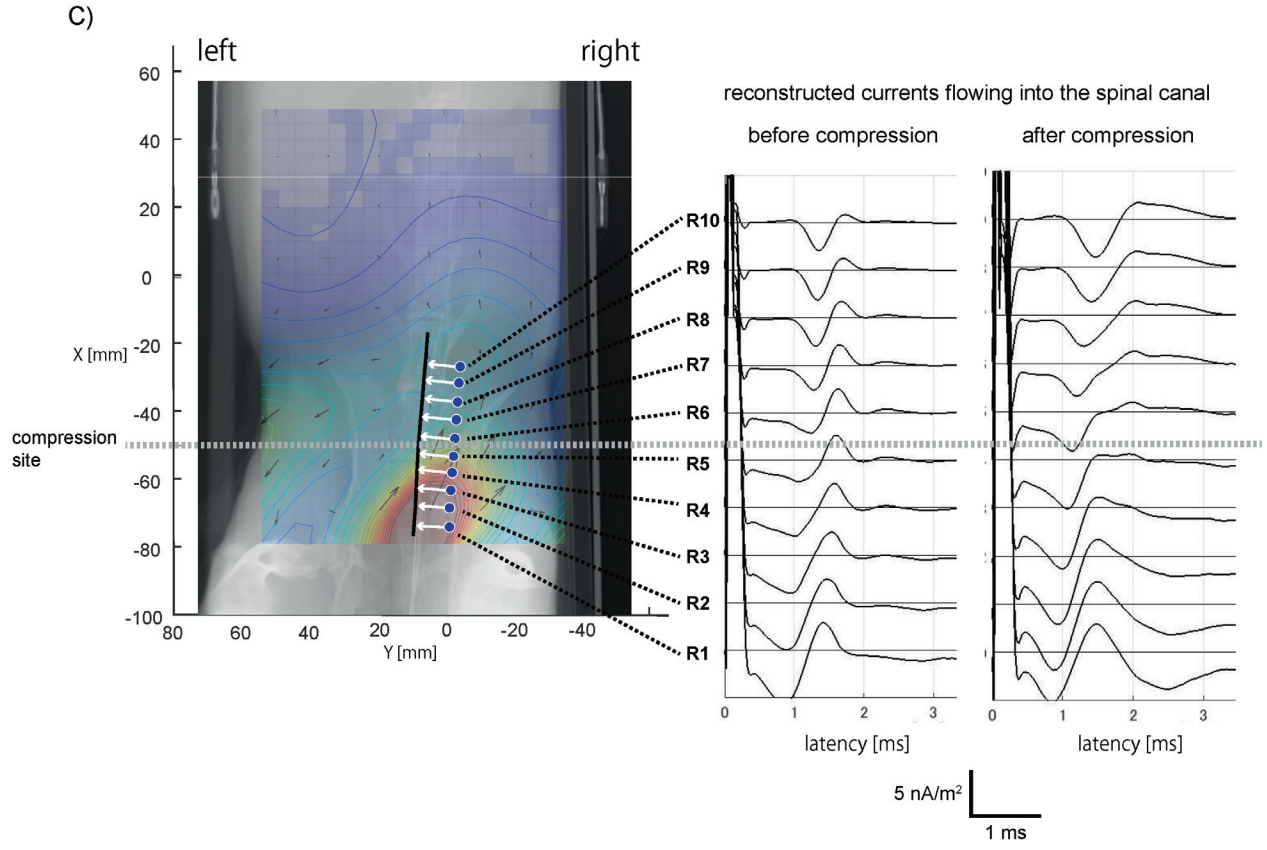

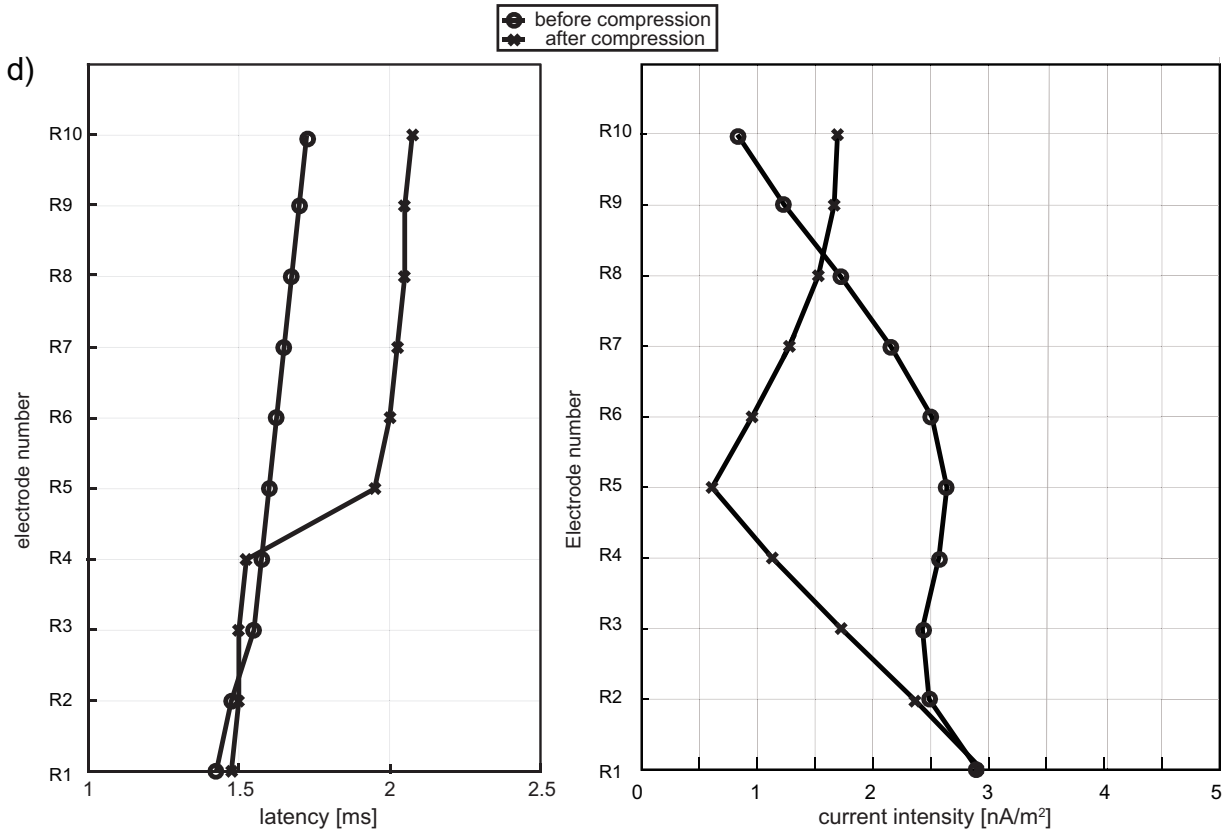

Fig. 8 (*continued*)

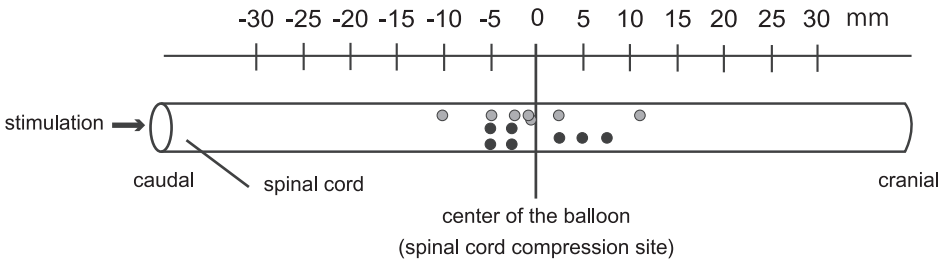

Fig. 9. Scatter plot of lesion sites estimated by LCEPs and reconstructed currents. In LCEPs, the lesion site is assumed to be the midpoint of two recording points where the peak amplitude decreased to less than 50% of the recording before the spinal compression. In reconstructed currents, the lesion sites are estimated by the change in the peak latency and the current density, as shown in Fig. 8d. Gray dots represent the lesion sites of the seven rabbits estimated by LCEPs and black dots represent those estimated by reconstructed currents. The caudal stimulation side is assumed to be negative in this scale, and the center of the balloon is set as zero. LCEP: lumbar canal evoked potential.

from coil Z represent magnetic fields generated mainly by intra-axonal currents (Supplementary Fig. S1). Before the spinal cord compression, the contour map of the Z coil showed the leading and trailing magnetic fields conducting in the caudal-to-cranial direction. However, the leading component of the magnetic field decelerated and was attenuated around the lesion site after the compression. In addition, the trailing component barely appeared at 2.0 ms (Fig. 7c). As we have reported in our previous studies of isolated peripheral nerves, the first component of magnetic fields generated by the leading intra-axonal current is attenuated around the lesion site. When the depolarization site reaches the lesion site, the trailing component or the trailing intra-axonal currents are also attenuated and disappear before the lesion site (Fukuoka et al., 2002, 2004).

The signals recorded from coil X were magnetic fields mainly caused by currents flowing into and out of the nerve (Supplementary Fig. S1c). Because the middle component of the LCEFs from coil X is generated by volume currents flowing into the depolarization site, the starred area in the isomagnetic contour map represents magnetic fields generated by such currents (Fig. 7a). These components are shown as a positive peak in Fig. 6e. The LCEFs from the depolarization site can be used for localization. We also analyzed these signals and estimated the positions of the lesions in the seven rabbits (mean ± SD, −2.33 ± 7.54 mm; n = 7). However, in this report, we presented the results of LCEPs and reconstructed currents to focus on the clinical application of MSG.

In this study, the amplitudes of LCEFs from X sensors were generally larger on the contralateral side of the stimulation (Fig. 6b). A similar phenomenon was observed in our previous studies with animal and human subjects (Ishii et al., 2012; Tomizawa et al., 2008). Because the conductive pathway from the peroneal nerve to the spinal cord is curved, it is possible that the LCEFs on the concave side (the stimulation side) cancel each other out. However, further research is needed to elucidate this phenomenon.

Before the spinal cord compression, the middle positive peak of the LCEFs representing the depolarization site was conducted in the caudal-to-cranial direction at a similar CV to that of the LCEPs (Figs. 5, 6b), although the mean CV of the LCEFs was higher than that of the LCEPs. After the compression, this positive peak of the LCEF from coil X decelerated or was attenuated near the lesion site (Fig. 6b and e).

In the seven rabbits, the lesion sites could be estimated by the LCEPs (gray dots in Fig. 9) and the currents reconstructed from LCEFs (black dots in Fig. 9). The means of the estimated lesion sites in the LCEPs and reconstructed currents were both within 1 mm (mean ± SD: LCEPs, −0.88 ± 6.10 mm; reconstructed currents, 0.0 0 ± 4.50 mm). These estimated lesion sites could not be statistically compared because the distances between the measurement points differed between LCEPs (15 mm) and LCEFs (5 mm). However, it can be concluded that the lesion sites could be estimated by reconstructed currents corresponding to a depolarization site to the similar extent as the LCEPs directly recorded from the epidural catheter electrode.

In the representative case shown in Figs. 6–9, the lesion sites estimated by the LCEPs and reconstructed currents were 11.06 mm and −2.5 mm, respectively. This was a case when the discrepancy between the center of the balloon and the estimated lesion site was the largest in LCEPs. It could be due to a broader interval of electrodes in LCEPs or the relative position of the balloon and the poles of the electrode. However, further research on the correspondence between LCEPs and LCEFs at the lesion site may be needed.

The currents reconstructed from the LCEFs also propagated in the caudal-to-cranial direction before the spinal cord compression (Fig. 8a) and decelerated and were attenuated around the lesion site after the compression (Fig. 8b). The reconstructed currents at the blue circles in Fig. 8c are currents flowing toward the spinal cord. Considering their directions, these are supposed to be currents flowing into the depolarization site. As shown in Fig. 9, the lesion sites can be estimated by the reconstructed currents at the blue circles within an error of 7.5 mm.

In some ways, it can be advantageous to record LCEFs rather than LCEPs. First, MSG can visualize neural activity as reconstructed currents. Although analysis of neural currents is difficult in traditional electrophysiological examinations, the visualization of conducting currents is sufficiently thorough for examiners not specialized in neurophysiology and may contribute to new neurological findings. Second, MSG does not need a contact sensor array nor an epidural electrode, in contrast to the recording of evoked potentials. As described in the Introduction, recording of LCEPs from an epidural electrode has been used because skin surface recording lacks accuracy. Therefore, we considered MSG, which is a less invasive and more efficient modality for functional examination of the spinal cord.

There have been a few pioneering reports on evoked magnetic fields in the lumbar region (Mackert et al., 1997, 1998; Klein et al., 2006). Mackert et al. (1997, 1998) used MNG to localize a conduction block in the S1 nerve root caused by an L5/S herniated disc. However, the evoked signals were about 10 fT and the estimated position was 2.5 cm more caudally to the lesion site. The results were not precise enough for clinical use, mainly due to limitations in the recording device and signal processing at the time of the experiment.

Although we have already reported LCEFs in animal and human subjects, the present study has some differences from our previous reports, besides improvements in the MSG device and signal processing methods. First, we have previously recorded LCEFs of healthy human subjects in response to peripheral nerve stimulation (Ishii et al., 2012; Sumiya et al., 2017), but we evaluated LCEFs with spinal cord compression in this study. Second, in previous studies, LCEFs recorded from the lumbar area contained magnetic fields from both propagating action currents and synaptic activities

in the dorsal horn (Ishii et al., 2012; Tomizawa et al., 2008). In this report, we used higher frequency stimulation to suppress synaptic activity, enabling easier observation of conducting neural activities mainly from the dorsal column (Seyal and Gabor, 1987). Third, we have reported the LCEFs of the cervical spinal cord of animals in response to stimulation of the lower thoracic spinal cord, recorded after cervical laminectomy (Kawabata et al., 2002) or from the skin surface (Tomori et al., 2010). In the present study, we used peripheral nerve stimulation, which is less invasive and can be clinically applied. In addition, the magnetic fields were measured from the intact skin surface.

While research in MSG has progressed and we have reported LCEFs of the cervical spinal cord in human subjects (Sumiya et al., 2017), there are still several topics to be elucidated to refine the clinical use of MSG; for example, magnetic fields generated by synaptic activity or the nerve plexus, an optimal and less invasive stimulation method. This study also has some limitations. Although the magnetic fields from synaptic activity were suppressed by higher frequency stimulation, the recorded magnetic fields contained the neural activities of both the lumbar spinal cord and cauda equina, considering the anatomy of the rabbit spinal cord (Greenaway et al., 2001; Sohn and Couto, 2012). Further study is needed to differentiate these combined signals. In addition, muscle relaxant was used and artifacts from muscle contraction were negligible in this study. However, the clinical use of this technique in human subjects necessitates less invasive stimulation and the artifact reduction method should be further improved.

5. Conclusions

In summary, MSG recorded at the skin surface can successfully visualize neural activity in the rabbit spinal cord and cauda equina in response to sciatic nerve stimulation. The position of the spinal cord compression site can be estimated by reconstructed currents from the depolarization site, with a similar precision to LCEPs from an epidural catheter electrode. This study provides further advances toward the clinical application of MSG.

Funding

This work was supported by a Grant-in-Aid for Scientific Research from the Ministry of Education, Culture, Sports, Science and Technology in Japan [grant number No. 19659376]. The funding source had no role in the study design; in the collection, analysis, or interpretation of data; in the writing of the report; or in the decision to submit the article for publication.

Declaration of Competing Interest

None of the authors has potential conflicts of interest to be disclosed.

Appendix A. Supplementary material

Supplementary data to this article can be found online at https://doi.org/10.1016/j.clinph.2020.02.025.

References

Adachi Y, Kawai J, Miyamoto M, Ogata H, Tomori M, Kawabata S, et al. A SQUID system for measurement of spinal cord evoked field of supine subjects. IEEE Trans Appl Supercond 2009;19:861–6. https://doi.org/10.1109/TASC.2009.2019199.

Erné SN, Narici L, Pizella V, Romani GL. The positioning problem in biomagnetic measurements: a solution for arrays of superconducting sensors. IEEE Trans Magn 1987;23:1319–22. https://doi.org/10.1109/TMAG.1987.1064889.

Fukuoka Y, Komori H, Kawabata S, Ohkubo H, Shinomiya K, Terasaki O. Imaging of neural conduction block by neuromagnetic recording. Clin Neurophysiol 2002;113:1985–92.

Fukuoka Y, Komori H, Kawabata S, Ohkubo H, Shinomiya K. Visualization of incomplete conduction block by neuromagnetic recording. Clin Neurophysiol 2004;115:2113–22. https://doi.org/10.1016/j.clinph.2004.03.033.

Greenaway JB, Partlow GD, Gonsholt NL, Fisher KR. Anatomy of the lumbosacral spinal cord in rabbits. J Am Anim Hosp Assoc 2001;37:27–34. https://doi.org/10.5326/15473317-37-1-27.

Hoshino Y, Kawabata S, Komori H, Ohkubo H, Tomizawa M, Shinomiya K. Three-dimensional neuromagnetic recording in the spinal cord. Int Congress Series 2005;1278:309–12. https://doi.org/10.1016/j.ics.2004.11.004.

Ishii S, Kawabata S, Tomizawa S, Tomori M, Sakaki K, Shinomiya K, et al. Conductive neuromagnetic fields in the lumbar spinal canal. Clin Neurophysiol 2012;123:1656–61. https://doi.org/10.1016/j.clinph.2011.12.014.

Kakigi R, Shibasaki H, Hashizume A, Kuroiwa Y. Short latency somatosensory evoked spinal and scalp-recorded potentials following posterior tibial nerve stimulation in man. Electroencephalogr Clin Neurophysiol 1982;53:602–11.

Kawabata S, Komori H, Mochida K, Harunobu O, Shinomiya K. Visualization of conductive spinal cord activity using a biomagnetometer. Spine 2002;27:475–9.

Klein A, van Leeuwen P, Hoormann J, Gronemeyer D. Magnetoneurographic registration of propagating magnetic fields in the lumbar spine after stimulation of the posterior tibial nerve. J Neural Eng 2006;3:125–31.

Kumihashi I, Sekihara K. Array-gain constraint minimum-norm spatial filter with recursively updated gram matrix for biomagnetic source imaging. IEEE Trans Biomed Eng 2010;57:1358–65. https://doi.org/10.1109/TBME.2010.2040735.

Mackert BM, Curio G, Burghoff M, Marx P. Mapping of tibial nerve evoked magnetic fields over the lower spine. Electroencephalogr Clin Neurophysiol 1997;104:322–7.

Mackert BM, Curio G, Burghoff M, Trahms L, Marx P. Magnetoneurographic 3D localization of conduction blocks in patients with unilateral S1 root compression. Electroencephalogr Clin Neurophysiol 1998;109:315–20.

Ohkubo H, Komori H, Kawabata S, Fukuoka Y, Shinomiya K. Estimation of localization of neural activity in the spinal cord using a biomagnetometer. J Med Dent Sci 2003;50:177–82.

Sarvas J. Basic mathematical and electromagnetic concepts of the biomagnetic inverse problem. Phys Med Biol 1987;32:11–22.

Sekihara K, Kawabata Y, Ushio S, Sumiya S, Kawabata S, Adachi Y, Nagarajan SS. Dual signal subspace projection (DSSP): a novel algorithm for removing large interference in biomagnetic measurements. J Neural Eng 2016;13. https://doi.org/10.1088/1741-2560/13/3/036007 036007.

Sekihara K, Nagarajan SS. Electromagnetic brain imaging. Cham: Springer International Publishing; 2015. https://doi.org/10.1007/978-3-319-14947-9.

Seyal M, Gabor AJ. Generators of human spinal somatosensory evoked potentials. J Clin Neurophysiol 1987;4:177–87. https://doi.org/10.1016/0013-4694(83)90210-9.

Sohn J, Couto MA. Anatomy, physiology and behavior. In: Suckow MA, Stevens KA, Wilson RP, editors. The laboratory rabbit, guinea pig, hamster, and other rodents. Academic Press; 2012. p. 195–215.

Stenroos M, Sarvas J. Bioelectromagnetic forward problem: isolated source approach revis(it)ed. Phys Med Biol 2012;57:3517–35. https://doi.org/10.1088/0031-9155/57/11/3517.

Sumiya S, Kawabata S, Hoshino Y, Adachi Y, Sekihara K, Tomizawa S, et al. Magnetospinography visualizes electrophysiological activity in the cervical spinal cord. Sci Rep 2017;7:2192. https://doi.org/10.1038/s41598-017-02406-8.

Tomizawa S, Kawabata S, Komori H, Hoshino Fukuoka Y, Shinomiya K. Evaluation of segmental spinal cord evoked magnetic fields after sciatic nerve stimulation. Clin Neurophysiol 2008;119:1111–8. https://doi.org/10.1016/j.clinph.2008.01.017.

Tomori M, Kawabata S, Tomizawa S, Ishii S, Enomoto M, Adachi Y, et al. Diagnosis of incomplete conduction block of spinal cord from skin surface using spinal cord evoked magnetic fields. J Orthop Sci 2010;15:371–80. https://doi.org/10.1007/s00776-010-1463-3.

Wijesinghe RS. Magnetic measurements of peripheral nerve function using a neuromagnetic current probe. Exp Biol Med (Maywood) 2010;235:159–69. https://doi.org/10.1258/ebm.2009.009306.

Yamada T, Machida M, Kimura J. Far-field somatosensory evoked potentials after stimulation of the tibial nerve. Neurology 1982;32:1151–8.

Yamada T. Neuroanatomic substrates of lower extremity somatosensory evoked potentials. J Clin Neurophysiol 2000;17:269–79.